Supplementary Information

Visualizing reactive astrocyte-neuron interaction in Alzheimer's disease using ^{11}C-acetate and ^{18}F-FDG

Min-Ho Nam†, Hae Young Ko†, Dongwoo Kim†, Sangwon Lee, Yongmin Mason Park, Seung Jae Hyeon, Woojin Won, Jee-In Chung, Seon Yoo Kim, Han Hee Jo, Kyeong Taek Oh, Young-Eun Han, Gwan-Ho Lee, Yeon Ha Ju, Hyowon Lee, Hyunjin Kim, Jaejun Heo, Mridula Bhalla, Ki Jung Kim, Jea Kwon, Thor D. Stein, Mingyu Kong, Hyunbeom Lee, Seung Eun Lee, Soo-Jin Oh, Joong-Hyun Chun, Mi-Ae Park, Ki Duk Park, Hoon Ryu*, Mijin Yun*, C. Justin Lee*

Supplementary Data

Supplementary Fig. 1 to 10

Supplementary Table 1 to 4

Original blots and gel images

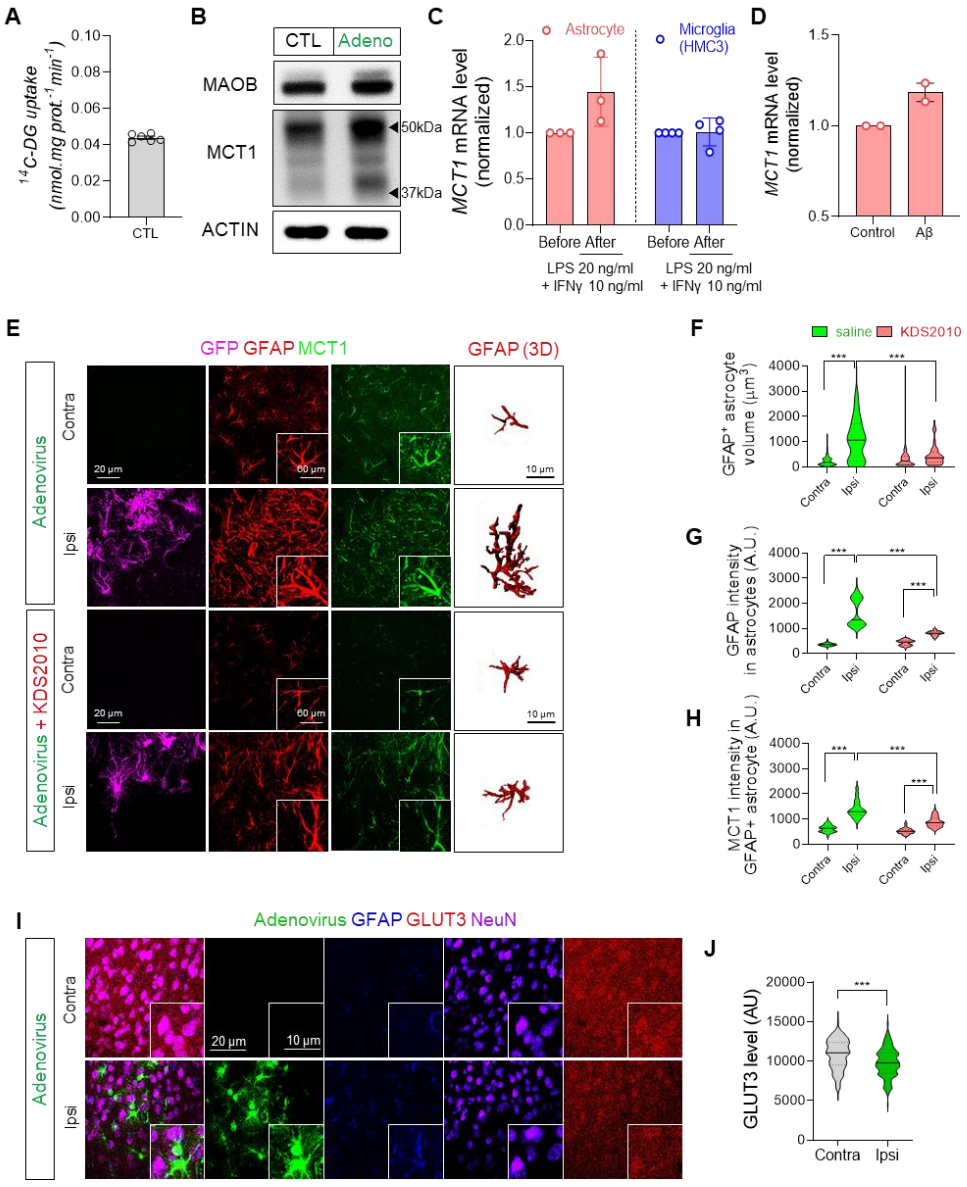

Supplemental Figure 1. The augmented astrocytic MCT1 and reduced neuronal GLUT3 under the condition of neuroinflammation.

(**A**) ^{14}C-DG uptake of primary astrocytes. (**B**) Western blotting of MAOB and MCT1 in adenovirus-treated (48-hour) reactive astrocytes. (**C**) MCT1 mRNA expression in LPS and IFNγ-induced (24-hour) reactive astrocytes and reactive microglia. (**D**) MCT1 mRNA expression in control and Aβ-treated (5-day) astrocytes. (**E**) Representative confocal images of rat cortical tissues and representative 3D-rendered GFAP-positive astrocytes. (**F**) Quantification of the volume of GFAP-positive astrocytes. Adenovirus increased the volume of GFAP-positive astrocytes, which was significantly attenuated by KDS2010 treatment (n = 117, 57, 115, and 75 cells from three rats for each group, respectively). (**G**) Quantification of the GFAP intensity in astrocytes. Adenovirus increased the GFAP intensity, which was significantly

attenuated by KDS2010 treatment (n = 117, 57, 115, and 75 cells from three rats for each group, respectively). (**H**) Quantification of the MCT1 immunoreactivity in astrocytes. Adenovirus increased the MCT1 immunoreactivity, which was significantly attenuated by KDS2010 treatment (n = 45, 61, 46, and 64 cells from three rats for each group, respectively). (**I**) Representative confocal images of rat cortical tissues demonstrating reduced GLUT3 expressions by adenovirus infection. (**J**) Quantification of GLUT3 expression (n = 722 and 815 cells from contralateral and ipsilateral cortex of three rats, respectively). Mean ± SEM for bar graphs. Median and quartiles for violin plots. Significance was assessed by Two-way ANOVA with Tukey (**F, G, H**) or two-tailed unpaired Student's t-test (**J**).

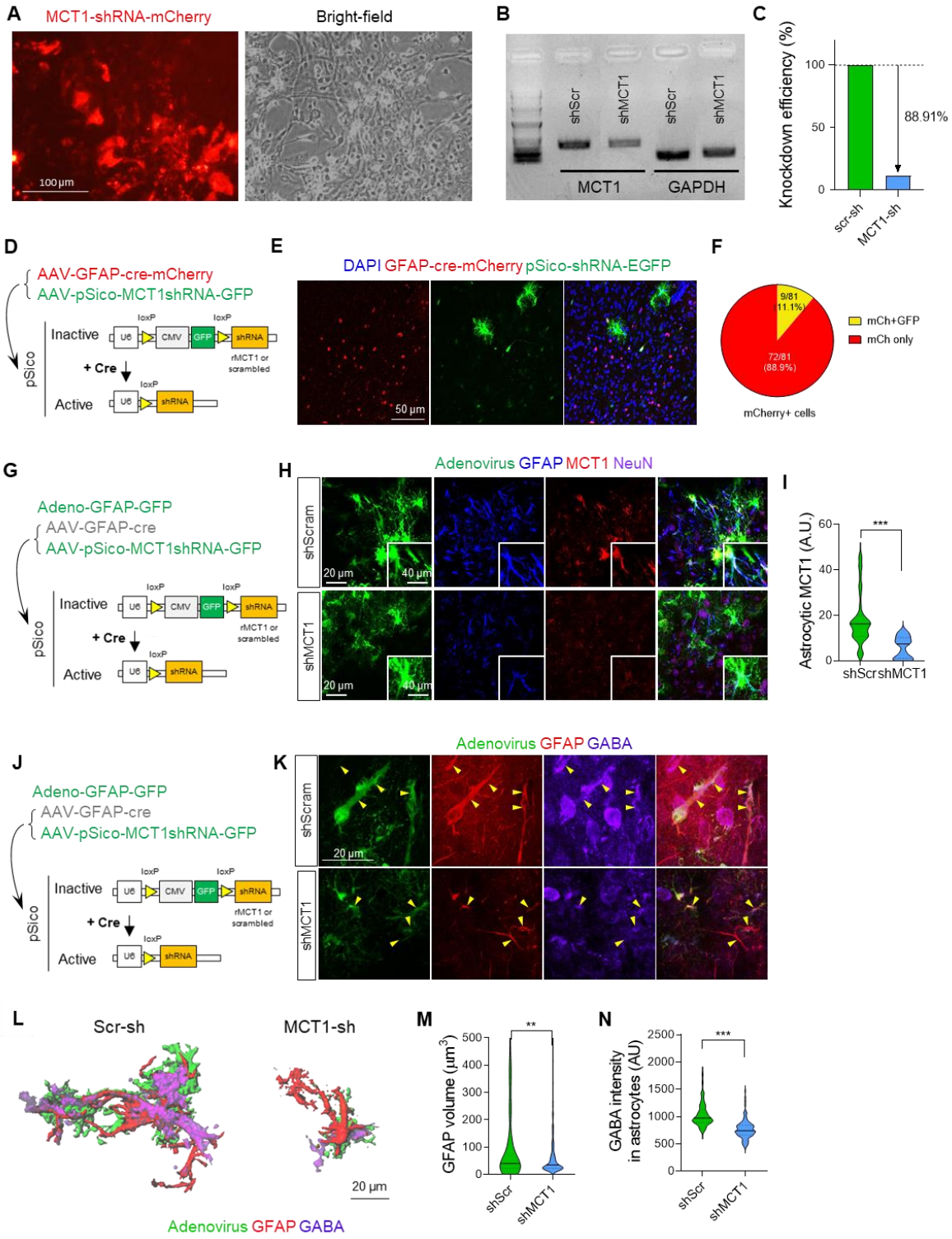

Supplemental Figure 2. Astrocyte-specific MCT1 gene silencing ameliorates reactive astrogliosis. (**A**) Representative images of primary cultured rat cortical astrocytes. (**B**) RT-PCR bands demonstrating MCT1-shRNA markedly reduced MCT1 expression. (**C**) Quantification of knockdown efficiency of MCT1 from qRT-PCR experiments. (**D, G, J**) Schematic diagram of astrocyte-specific *Mct1* knockdown

strategies. (**E**) Representative confocal images of rat cortex. (**F**) Quantification of the Cre-dependent cleavage of EGFP signal in Cre-positive cells (n = 81 cells from three mice). (**H**) Representative confocal images of rat cortical tissues demonstrating reduced MCT1 expressions in the MCT1-shRNA-expressed astrocytes (n = 44 and 38 cells from three mice, respectively). (**I**) Quantification of MCT1 expression in astrocytes. (**K**) Representative confocal images of rat cortical tissues demonstrating reduced GFAP and GABA expressions in the MCT1-shRNA-expressed astrocytes. (**L**) Representative 3D-rendered astrocytes-expressing adeno-GFAP-GFP virus, GFAP, and GABA. (**M**) Quantification of GFAP-positive volume of each astrocyte (n = 68 and 117 cells from three mice, respectively). (**N**) Quantification of GABA expression in each astrocyte (n = 68 and 117 cells from three mice, respectively). Median and quartiles for violin plots. Significance was assessed by two-tailed unpaired Student's t-test.

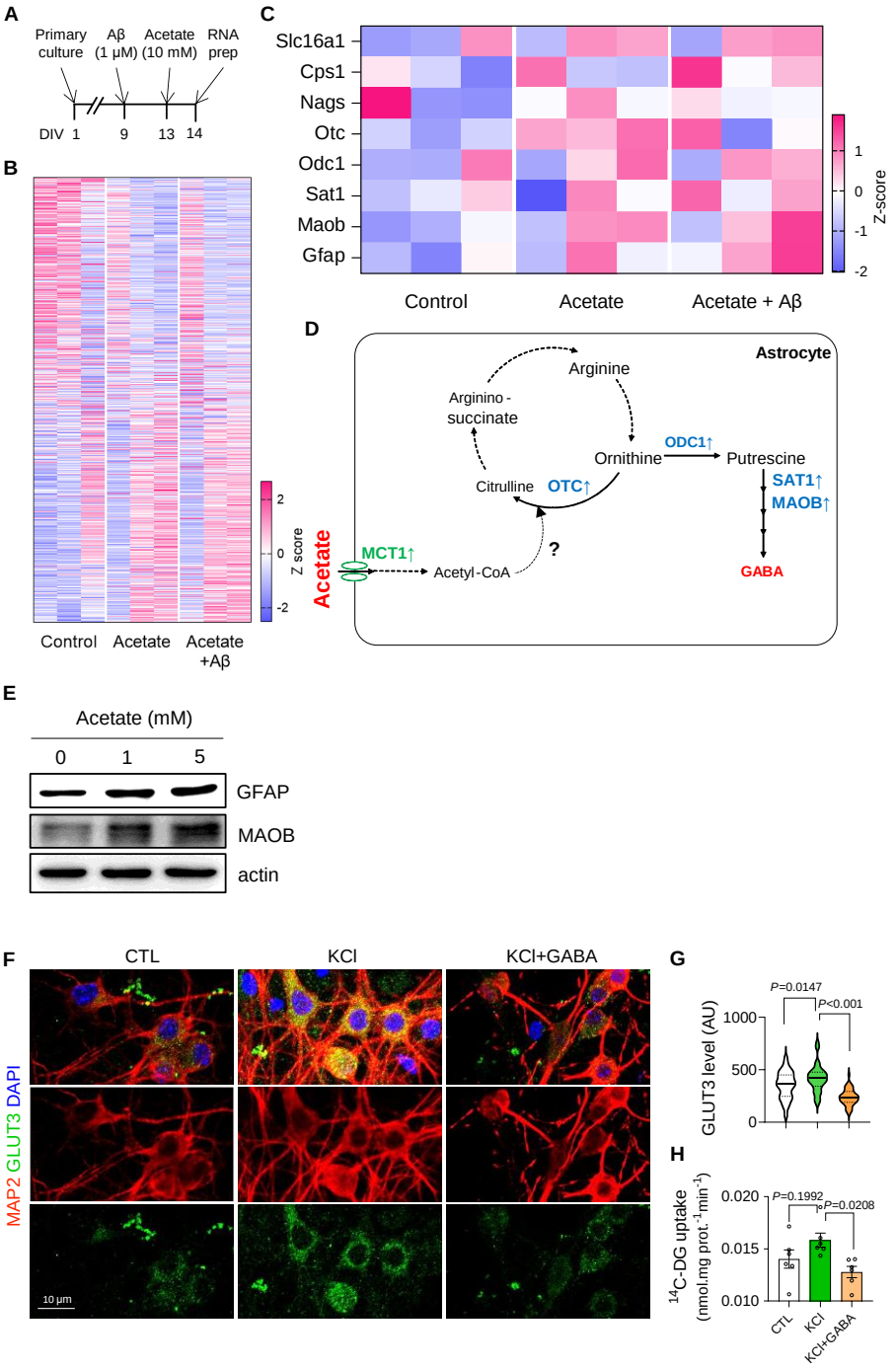

Supplemental Figure 3. Acetate boosts astrocytic urea cycle and subsequent GABA synthesis

(**A**) Experimental schedule of RNA-sequencing with primary cultured cortical astrocytes (n = 3 biological replicates for each condition). On DIV 13, the culture media was exchanged to glucose-free and serum-free media then treated with sodium acetate (10 mM) for 24 hours and Aβ (1 μM) for 5 days. (**B**) Heatmap of the expression of all genes for control, acetate-treated, and acetate and Aβ-treated group. (**C**) Heatmap of z-scores calculated from count per million (CPM) values of *Slc16a1, Cps1, Nags, Otc, Odc1,*

Sat1, Maob, and *Gfap* which are related to astrocytic GABA synthesis from urea cycle or astrocytic reactivity. (**D**) Schematic diagram of astrocytic GABA synthetic pathway which are upregulated by acetate treatment (highlighted in blue). (**E**) Western blotting of GFAP and MAOB in reactive astrocytes treated with sodium acetate (1 mM and 5 mM) for 2 days. (**F**) Representative immunocytochemical images of MAP2, GLUT3, and DAPI in primary cultured cortical neurons treated with KCl (20 mM, 20 mins) and GABA (100 μM, 24 hrs). (**G**) Quantification of GLUT3 immunoreactivity. (**H**) Quantification of ^{14}C-DG uptake in primary cultured cortical neurons treated with KCl and GABA, assessed by liquid scintillation counting of beta-particles. Mean ± SEM for bar graphs. Median and quartiles for violin plots. Significance was assessed by One-way ANOVA with Tukey (**G, H**).

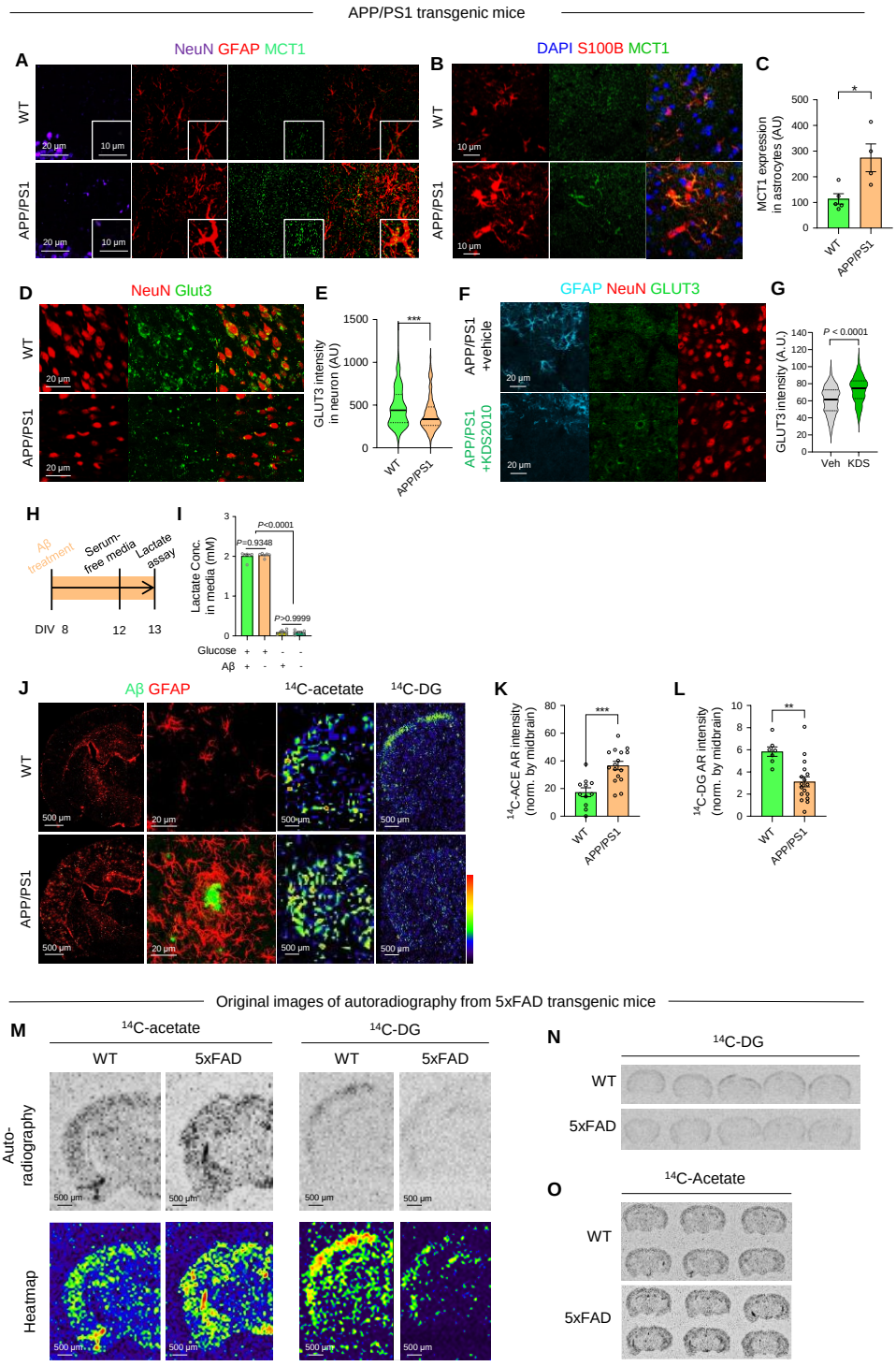

Supplemental Figure 4. MCT1 level and acetate uptake is increased, while GLUT3 level and glucose uptake is decreased in APP/PS1 and 5xFAD transgenic mice.

(**A, B**) Representative confocal images of APP/PS1 mouse cortical tissues demonstrating increased astrocytic (GFAP$^+$ or S100B$^+$) MCT1 expressions. (**C**) Quantification of GFAP-positive astrocytic MCT1

expression (each dot represents the average intensity of astrocytic MCT1 expression in a slice from each mouse). (**D**) Representative confocal images of APP/PS1 mouse cortical tissues demonstrating decreased neuronal GLUT3 expressions (n = 221 and 234 cells from three mice for each group, respectively). (**E**) Quantification of neuronal GLUT3 expression. (**F**) Representative confocal images of cortical tissue of APP/PS1 transgenic mice treated with KDS2010 (10 mg/kg/day) or vehicle. (**G**) Quantification of GLUT3 level in neurons. (**H**) Experimental schedule of lactate assay with Aβ-treated primary cultured cortical astrocytes under presence or absence of glucose. (**I**) Quantification of lactate concentration of the culture media harvested from the Aβ-treated astrocytes. The levels of lactate released from astrocytes were not affected by Aβ treatment, but significantly affected by absence of glucose. Aβ treatment, which increases astrocytic MCT1 expression, does not alter lactate release, suggesting that the increased MCT1 expression does not mediate lactate release. (**J**) Left, representative confocal images of Aβ and GFAP in APP/PS1 transgenic mice and the littermates. Right, representative autoradiography images of ^{14}C-acetate and ^{14}C-DG. (**K**) Quantification of ^{14}C-acetate intensity from autoradiography images (n = 11 and 16 slices from three mice for each group). (**L**) Quantification of ^{14}C-DG intensity from autoradiography images (n = 7 and 17 slices from three mice for each group). (**M**) Representative autoradiography images of ^{14}C-acetate and ^{14}C-DG in 5xFAD transgenic mice and the littermates. (**N, O**) Original autoradiography images of ^{14}C-acetate and ^{14}C-DG in 5xFAD transgenic mice and the littermates. Mean ± SEM for bar graphs. Median and quartiles for violin plots. Significance was assessed by two-tailed unpaired Student's t-test (**B, G, I, K, L**), or Two-way ANOVA with Tukey (**D**).

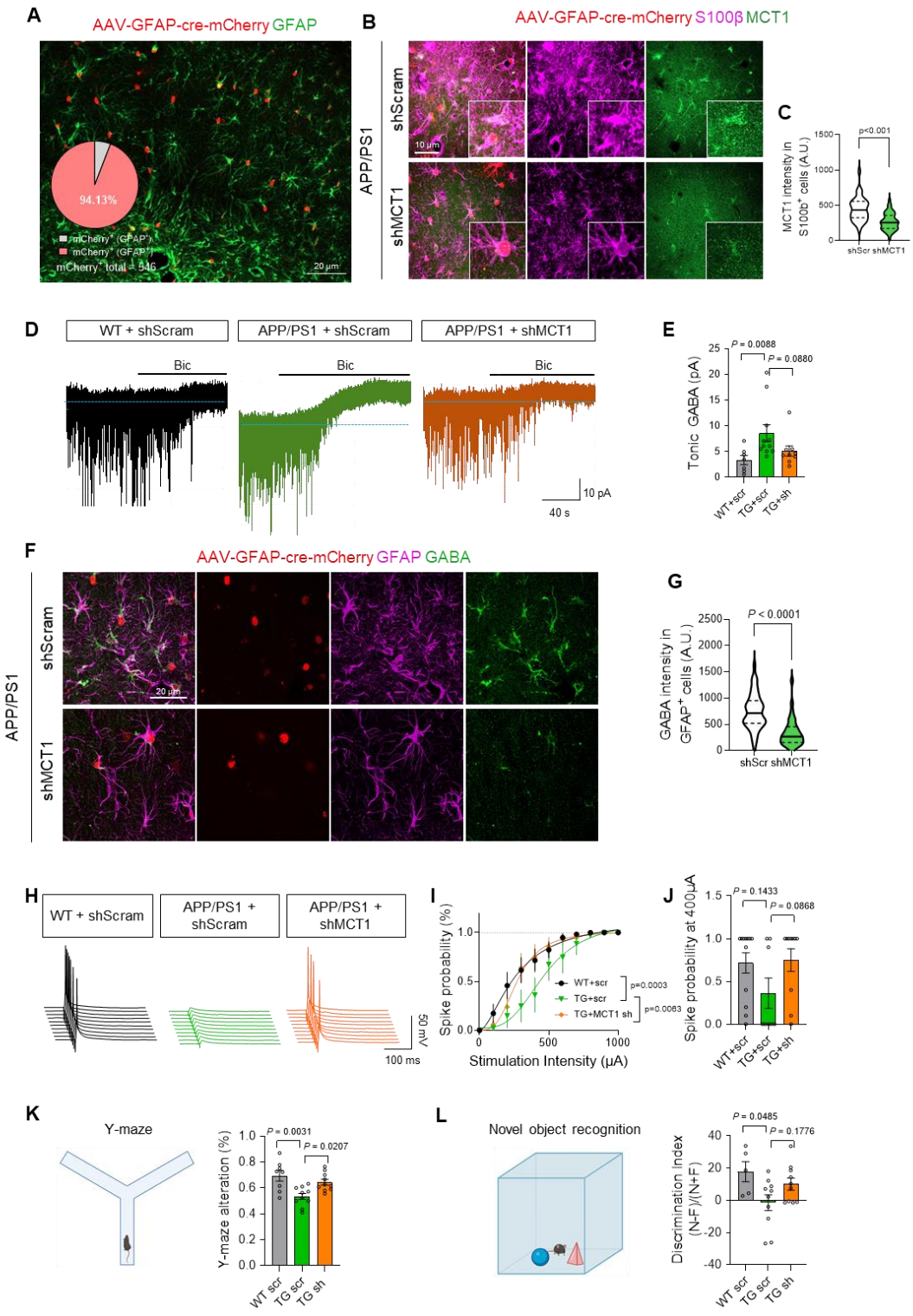

Supplemental Figure 5. Astrocyte-specific MCT1 gene-silencing reduces aberrant tonic inhibition and astrocytic GABA level, and rescues spike probability and memory impairment.

(**A**) Representative confocal images of AAV-GFAP-cre-mCherry and GFAP in APP/PS1 transgenic mice. Inset, Quantification of astrocyte specificity AAV-GFAP-cre-mCherry. (**B**) Representative confocal images of AAV-GFAP-cre-mCherry, S100b. and MCT1 in the hippocampus of APP/PS1 transgenic mice. (**C**) Quantification of S100b-positive astrocytic MCT1 expression (n = 34 and 47 cells from three mice for each group). (**D**) Representative traces of tonic GABA current recording from dentate granule cells in APP/PS1 transgenic mice with or without Astrocyte-specific MCT1 gene-silencing (n = 7, 11, and 9 cells from 4 mice for each group). (**E**) Quantification of tonic GABA current. (**F**) Representative confocal images of AAV-GFAP-cre-mCherry, GFAP, and GABA in the hippocampus of APP/PS1 transgenic mice with or without Astrocyte-specific MCT1 gene-silencing. (**G**) Quantification of GABA intensity in GFAP-positive astrocytes (n = 49 and 34 cells from three mice for each group). (**H**) Representative traces of spike probability recording from dentate granule cells upon electrical stimulation at performant path. (**I**) Quantification of spike probability upon various stimulation intensities. (**J**) Quantification of spike probability at 400 μA stimulation (n = 12, 8, and 10 cells from 4 mice for each group). (**K**) Assessment of memory function of APP/PS1 transgenic mice with or without Astrocyte-specific MCT1 gene-silencing by quantification of Y-maze alteration (N = 8, 10, and 10 mice for each group). (**L**) Assessment of memory function APP/PS1 transgenic mice with or without Astrocyte-specific MCT1 gene-silencing by quantification of discrimination index from novel object recognition test (N = 5, 10, and 10 mice for each group). Mean ± SEM for bar graphs. Median and quartiles for violin plots. Significance was assessed by two-tailed unpaired Student's t-test (**C, G**), one-way Kruskal-Wallis test with Duun (**E, J**), or one-way ANOVA with Tukey (**K, L**).

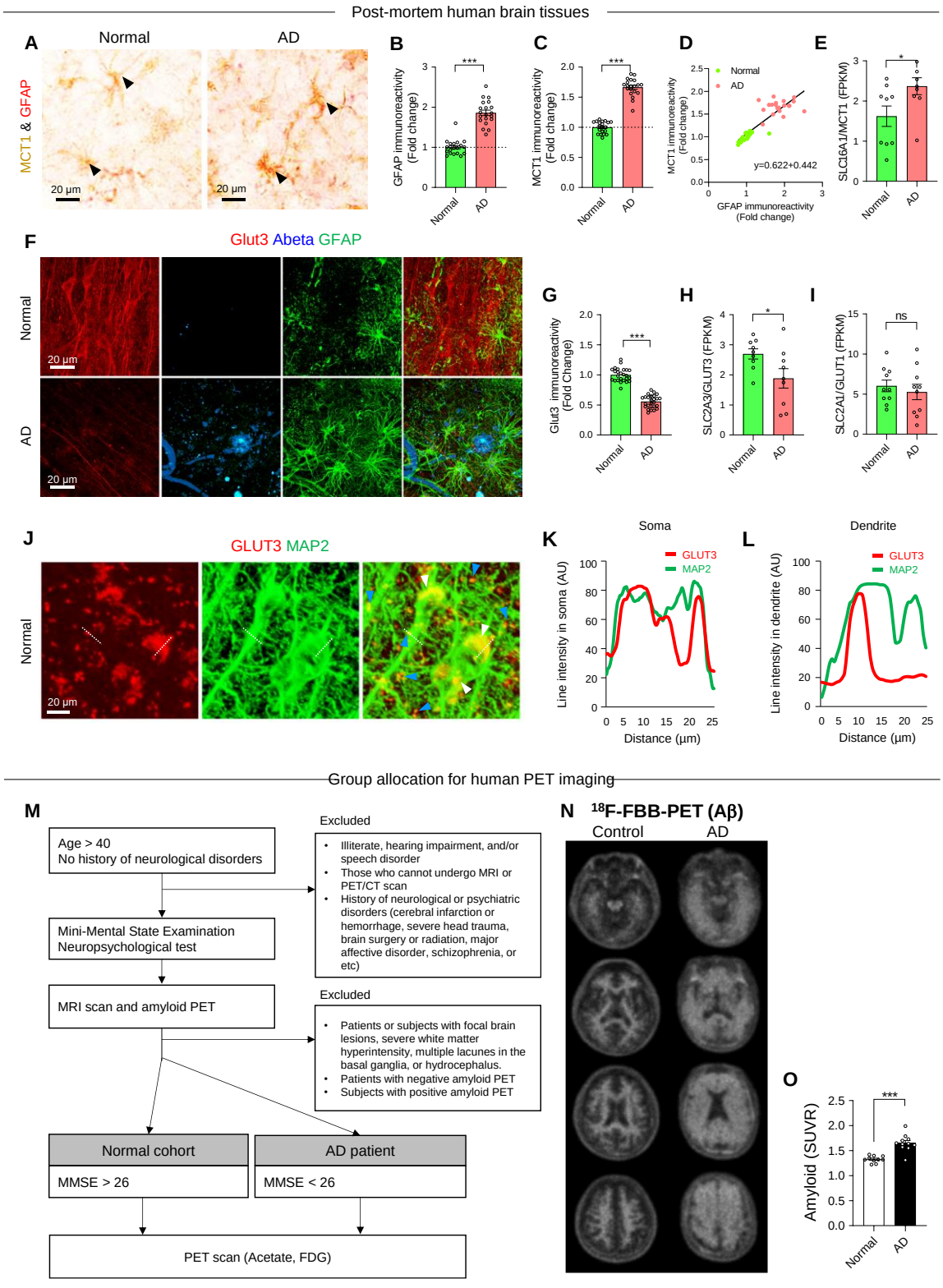

Supplemental Figure 6. MCT1 and GLUT3 expression in human postmortem tissue and group allocation for human PET imaging

(**A**) Representative images of human post-mortem forebrain tissues double-immunostained with MCT1 and GFAP. (**B**) Quantification of GFAP immunoreactivity. (**C**) Quantification of MCT1 immunoreactivity. (**D**) A positive correlation between MCT1 and GFAP immunoreactivities. (**E**) *SLC16A1* mRNA (encoding MCT1) expression in the frontal cortex of normal subjects and AD patients. (**F**) Representative images of human post-mortem forebrain tissues immunostained with GLUT3 and GFAP. (**G**) Quantification of GLUT3 immunoreactivity. (**H, I**) *SLC2A3* mRNA (encoding GLUT3) and *SLC2A1* mRNA (encoding GLUT1) expressions in the frontal cortex of normal subjects and AD patients. (**J**) Representative images of GLUT3 (red) and MAP2 (green) double-staining in the cortex of postmortem brain of normal subject. White and blue arrowheads indicate the colocalization of GLUT3 (red) and MAP2 (green) in both soma and dendrite processes of neurons, respectively. (**K, L**) Co-localization analysis of GLUT3 and MAP2 signals in the soma and the dendrite of neurons. White dotted lines in merged images indicate colocalization foci of GLUT3 and MAP2 signals. (**M**) Human subject selection criteria and selection procedure. (**N**) Representative brain ^{18}F-FBB-PET images of Aβ in control subjects and AD patients. (**O**) SUVR of Aβ in control subjects and AD patients. Mean ± SEM for bar graphs. Significance was assessed by two-tailed unpaired Student's t-test.

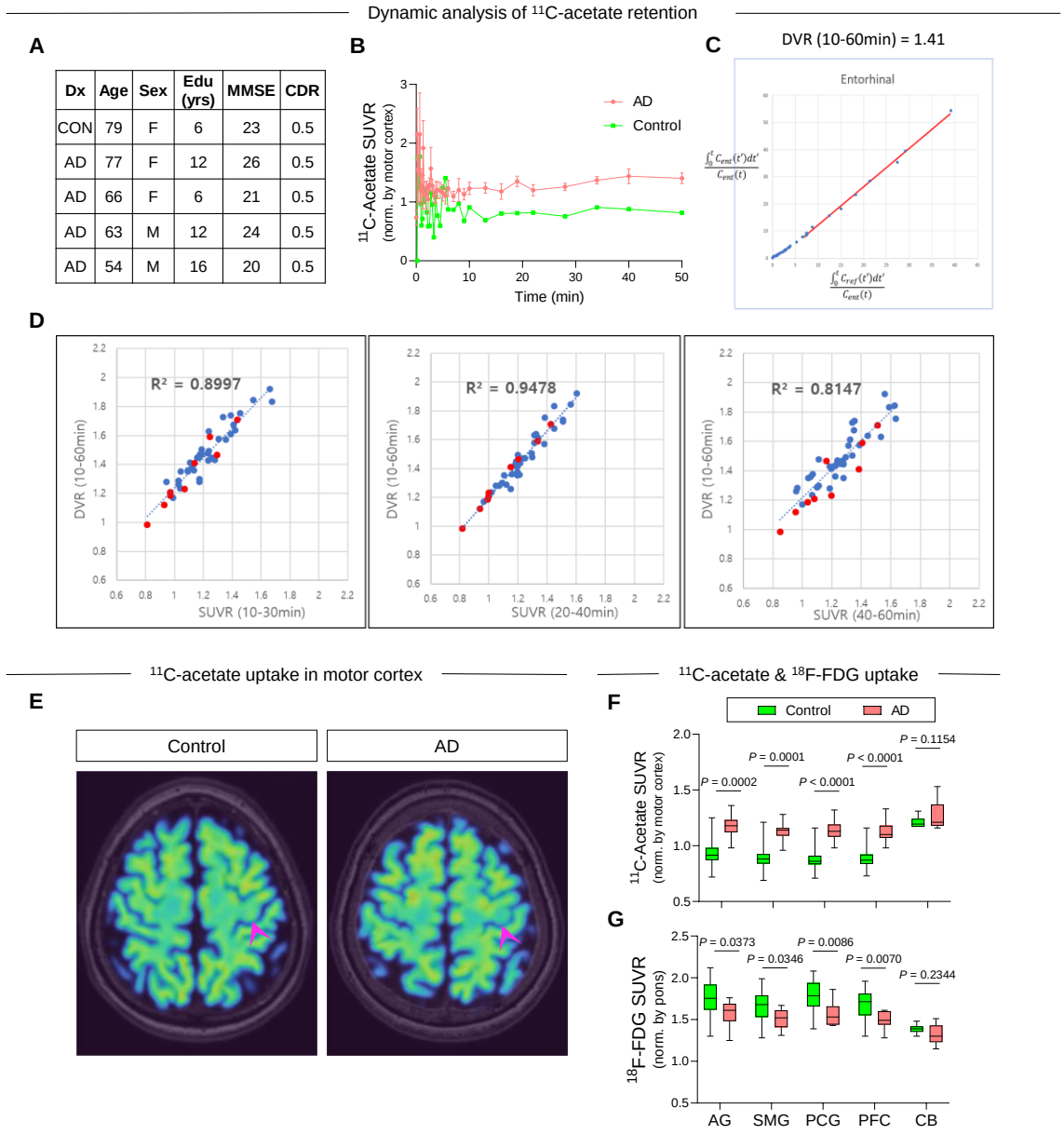

Dx	Age	Sex	Edu (yrs)	MMSE	CDR
CON	79	F	6	23	0.5
AD	77	F	12	26	0.5
AD	66	F	6	21	0.5
AD	63	M	12	24	0.5
AD	54	M	16	20	0.5

Supplemental Figure 7. Dynamic analysis ^{11}C-acetate retention and quantification of ^{11}C-acetate and ^{18}F-FDG SUVR in various brain regions

(**A**) Detailed information on the human subjects for dynamic analysis of ^{11}C-acetate retention. (**B**) Time-activity curve of ^{11}C-acetate in entorhinal cortex. AD patients showed higher ^{11}C-acetate SUVR than normal control subjects. Please note that the curves are stabilized within 10 min from tracer injection in both AD and normal subjects. (**C**) Distribution volume ratio (DVR) of ^{11}C-acetate in the entorhinal cortex, which is calculated from time-activity curve (**B**). (**D**) The correlation between DVR and SUVR of ^{11}C-acetate in the entorhinal cortex at three different time-points (10-30 min, 20-40 min, and 40-60 min from tracer injection). (**E**) ^{11}C-acetate PET image in the motor cortex of control and AD subjects (indicated with pink arrowheads). (**F**) Quantification of ^{11}C-acetate SUVR in the angular gyrus, supramarginal gyrus,

posterior cingulate gyrus, prefrontal cortex, and cerebellar cortex of AD patients and normal subjects. (**G**) Quantification of ^{18}F-FDG SUVR in the angular gyrus (AG), supramarginal gyrus (SMG), posterior cingulate gyrus (PCG), prefrontal cortex (PFC), and cerebellar cortex (CB) of AD patients and normal subjects. Except for cerebellar cortex, there were significant increases in ^{11}C-acetate SUVR and significant decreases in ^{18}F-FDG SUVR in every ROI. Error bars indicate min to max for Box and whisker. Significance was assessed by two-tailed unpaired Student's t-test.

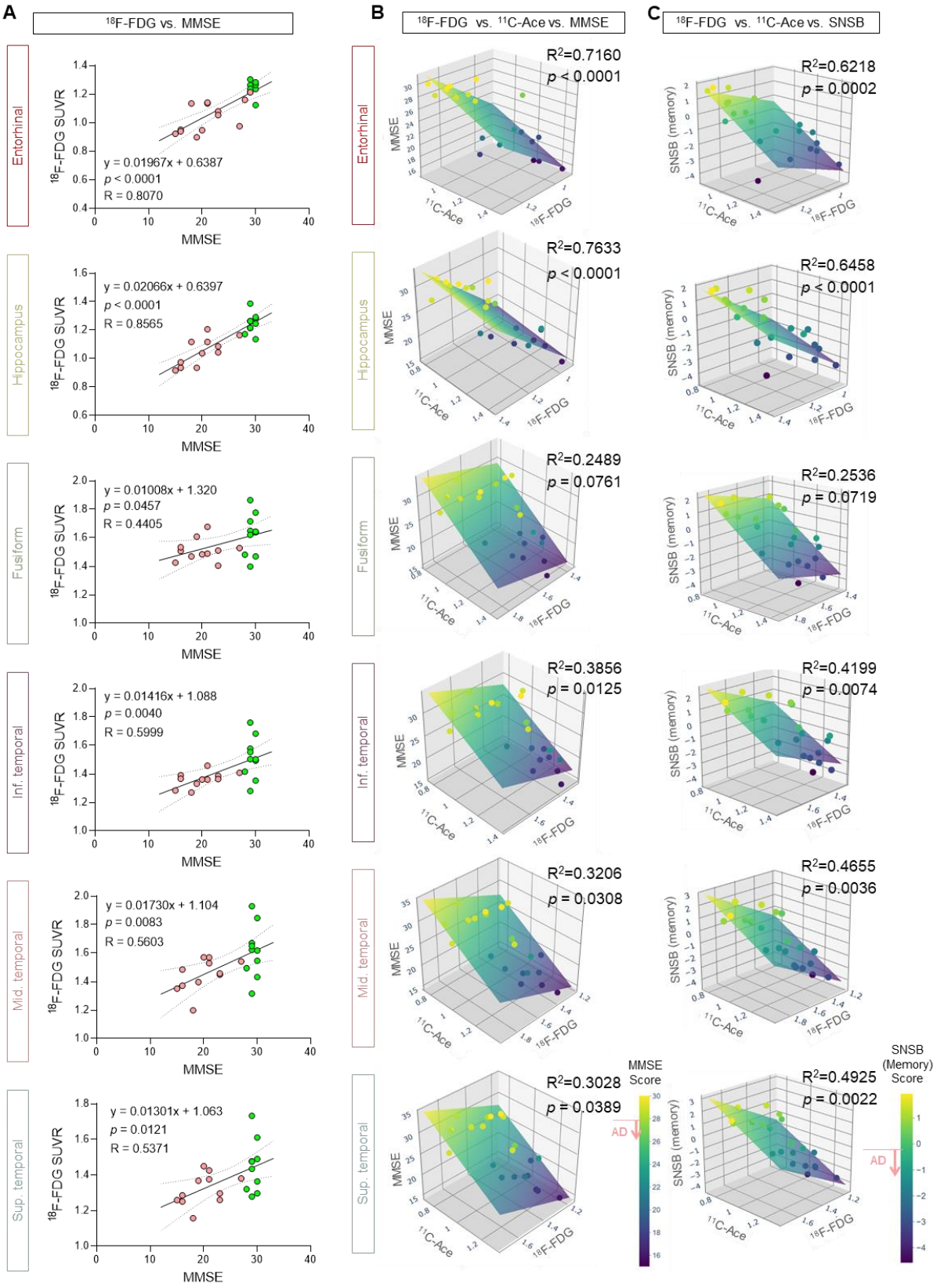
A
18F-FDG vs. MMSE
Entorhinal
y = 0.01967x + 0.6387
p < 0.0001
R = 0.8070
Hippocampus
y = 0.02066x + 0.6397
p < 0.0001
R = 0.8565
Fusiform
y = 0.01008x + 1.320
p = 0.0457
R = 0.4405
Inf. temporal
y = 0.01416x + 1.088
p = 0.0040
R = 0.5999
Mid. temporal
y = 0.01730x + 1.104
p = 0.0083
R = 0.5603
Sup. temporal
y = 0.01301x + 1.063
p = 0.0121
R = 0.5371
18F-FDG SUVR
MMSE
B
18F-FDG vs. 11C-Ace vs. MMSE
Entorhinal
R2=0.7160
p < 0.0001
Hippocampus
R2=0.7633
p < 0.0001
Fusiform
R2=0.2489
p = 0.0761
Inf. temporal
R2=0.3856
p = 0.0125
Mid. temporal
R2=0.3206
p = 0.0308
Sup. temporal
R2=0.3028
p = 0.0389
MMSE
11C-Ace
18F-FDG
C
18F-FDG vs. 11C-Ace vs. SNSB
Entorhinal
R2=0.6218
p = 0.0002
Hippocampus
R2=0.6458
p < 0.0001
Fusiform
R2=0.2536
p = 0.0719
Inf. temporal
R2=0.4199
p = 0.0074
Mid. temporal
R2=0.4655
p = 0.0036
Sup. temporal
R2=0.4925
p = 0.0022
SNSB (memory)
MMSE Score
SNSB (Memory) Score
AD

Supplemental Figure 8. Correlations between ^{18}F-FDG SUVR, ^{11}C-acetate SUVR, and memory function.

(**A**) Correlations between ^{18}F-FDG SUVR and MMSE score in entorhinal cortex, hippocampus, fusiform, inferior, middle, and superior temporal gyrus. In every ROI, significant positive correlations were observed between ^{18}F-FDG SUVR and MMSE score. (**B**) The multiple linear regression analysis showed that ^{18}F-FDG SUVR and ^{11}C-acetate SUVR has marked correlations with MMSE scores. (**C**) The multiple linear regression analysis showed that ^{18}F-FDG SUVR and ^{11}C-Acetate SUVR has marked correlations with SNSB (memory) scores. Significance was assessed by linear regression (**A**) or multiple linear regression with Pearson's correlation (**B, C**).

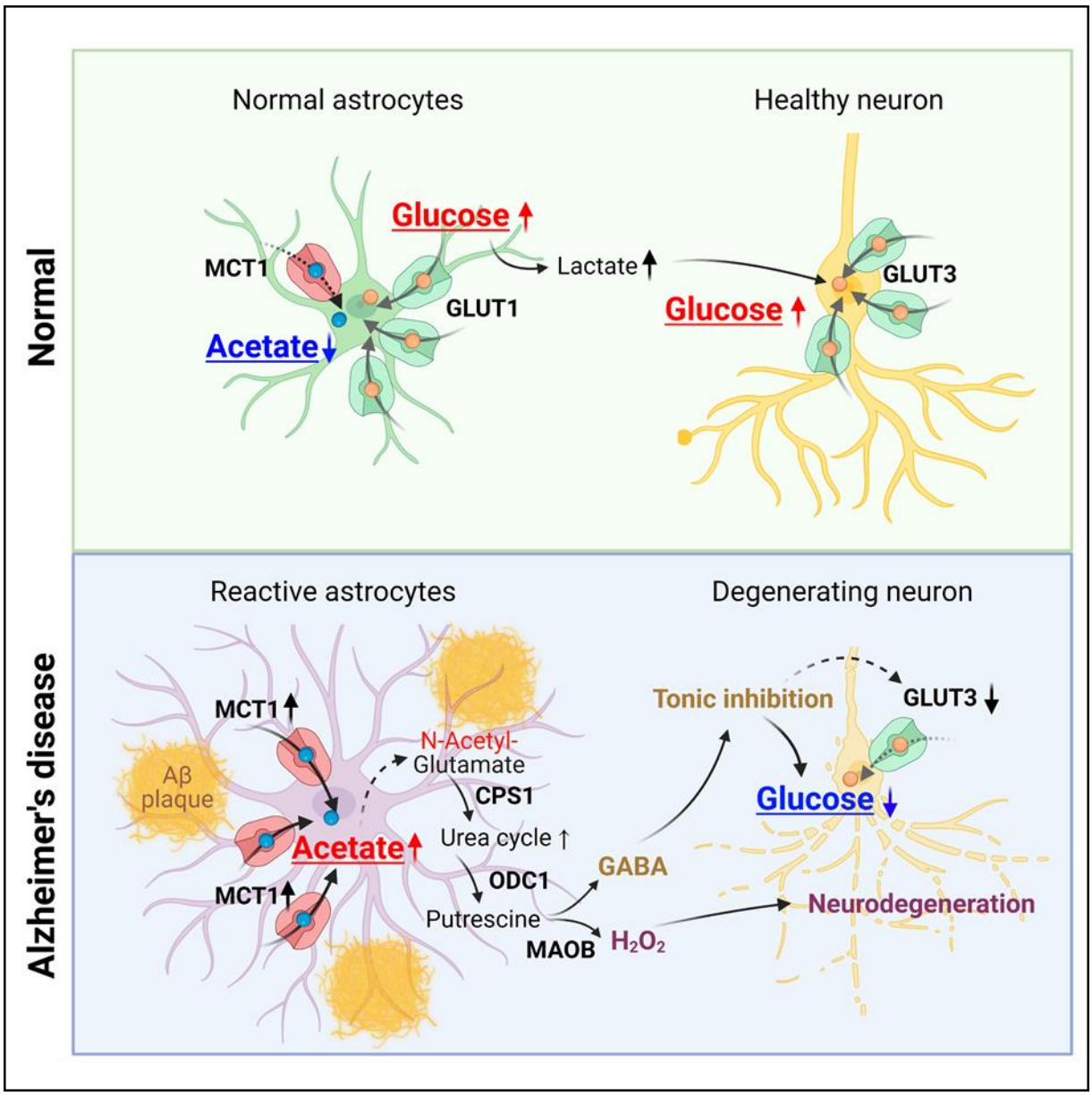

Supplemental Figure 9. Summary of working hypothesis about astrocyte-hypermetabolism and the associated neuronal-hypometabolism in AD brain.

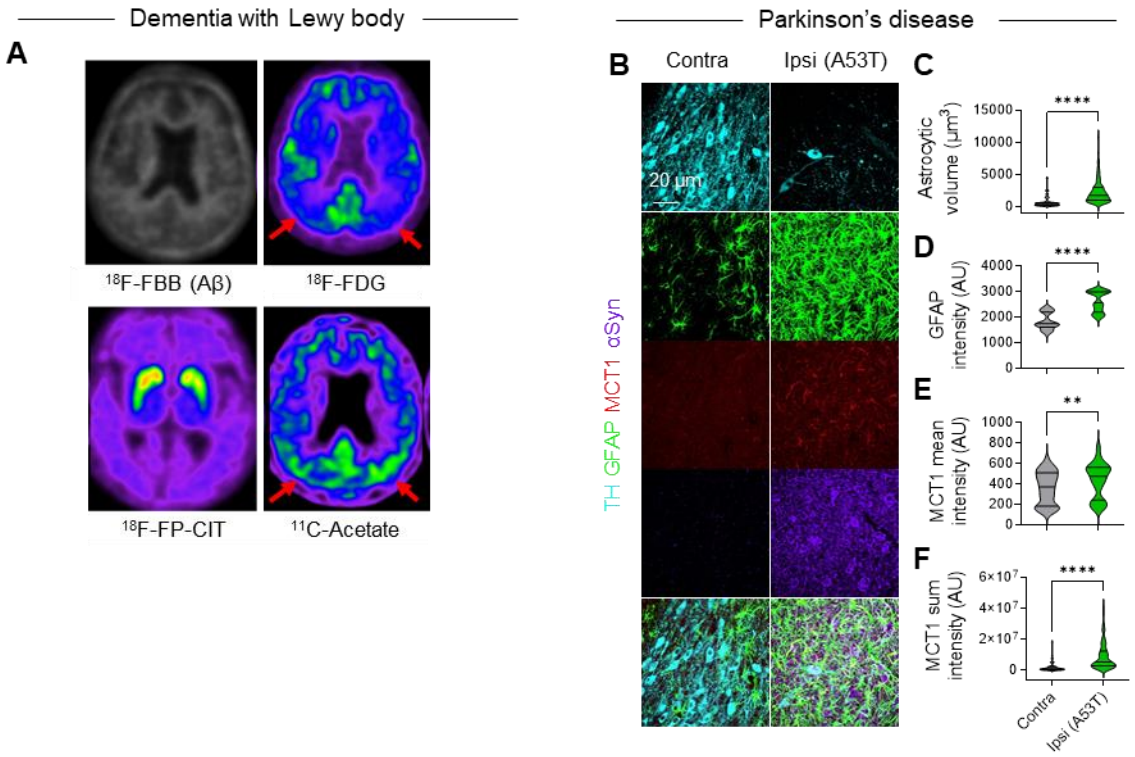

Supplemental Figure 10. Correlations between ^{18}F-FDG SUVR, ^{11}C-acetate SUVR, and memory function and proof-of-concept in other neurodegenerative disorders.

(**A**) Amyloid, FP-CIT, FDG, and acetate PET imaging of a patient with Lewy Body Dementia. Red arrows indicate the increased acetate uptake and decreased glucose uptake. (**B**) Representative confocal images of SNpc tissue from mouse PD models induced by viral overexpression of A53T-mutated alpha-synuclein (n = 54 and 102 cells from three mice for each group). (**C**) Quantification of astrocytic volume in the ipsilateral and contralateral SNpc. (**D**) Quantification of GFAP mean intensity. (**E**) Quantification of MCT1 mean intensity in GFAP-positive astrocytes. (**F**) Quantification of MCT1 sum intensity in GFAP-positive astrocytes. Median and quartiles for violin plots. Significance was assessed by two-tailed unpaired Student's t-test.

Supplemental Table 1. Information on postmortem brain tissue samples from normal subjects and AD patients.

Number	Case	Age	Sex	Braak stage
1	Normal	87	Female	I
2	Normal	88	Male	I
3	Normal	87	Female	II
4	Normal	67	Male	I
5	Normal	82	Male	I
6	Normal	78	Female	I
7	Normal	70	Male	I
8	Normal	82	Male	I
9	Normal	79	Female	I
10	Normal	80	Female	I
1	AD	85	Male	V
2	AD	87	Female	V
3	AD	82	Male	V
4	AD	79	Female	VI
5	AD	70	Male	VI
6	AD	80	Female	V
7	AD	75	Male	V
8	AD	83	Male	VI
9	AD	79	Female	VI
10	AD	69	Male	VI

Supplemental Table 2. Overall information on human subjects for PET/CT imaging study

(Mean ± SD)

		Control	AD	*p*
n		10	11	
Demographics				
	Age, yr	69.00 ± 10.49	74.45 ± 6.79	0.169
	Sex, female (%)	2 (20)	7 (63.64)	0.046
	Education, yr	13.00 ± 4.00	8.18 ± 4.71	0.021
Amyloid positivity, n		0	11	
Neuropsychological tests (SNSB)				
	Attention function	0.75 ± 1.02	-0.85 ± 0.75	<0.001
	Language function	3.72 ± 2.06	-0.88 ± 0.79	<0.001
	Visuospatial function	0.64 ± 0.73	-1.10 ± 1.32	0.002
	Memory function	0.75 ± 0.68	-2.35 ± 1.08	<0.001
	Frontal/executive function	1.05 ± 1.01	-2.03 ± 1.56	<0.001
K-MMSE score		29.30 ± 0.67	19.45 ± 3.50	<0.001
CDR-SOB		0.00 ± 0.00	0.73 ± 0.26	<0.001

Supplemental Table 3. Detailed information on human subjects for PET/CT imaging study

No	Dx	Age	Sex		Education (yrs)	MMSE	CDR	Attention	Language	Visuo-spatial Function	Memory	Frontal/ Executive Function
1	AD	80	F		6	16	1	-1.7	-1.51	-0.79	-2.7	-1.36
2	AD	81	M		16	23	0.5	-0.46	-0.13	0.09	-2.85	-0.46
3	AD	77	M		9	15	1	-0.67	-0.32	-2.13	-1.71	-0.97
4	AD	81	F		8	18	1	0.61	-1.03	-3.26	-2.97	-4.22
5	AD	72	F		6	16	1	-1.55	-1.3	-1.1	-3.23	-3.82
6	AD	81	M		0	21	0.5	-0.37	-2.34	-1.42	-0.81	-2.54
7	AD	73	F		6	19	0.5	-1.42	0.03	-0.37	-2.51	0.21
8	AD	69	F		10	21	0.5	-0.13	0.21	-3.03	-1.82	-3.57
9	AD	68	F		12	27	0.5	-1.68	-0.57	0.87	-1.48	-1.54
10	AD	77	F		3	20	0.5	-0.59	-1.515	0.31	-1.23	-0.55
11	AD	60	M		14	18	1	-1.39	-1.165	-1.29	-4.58	-3.52
12	Control	65	M		16	29	0	-0.48	5.53	0.63	0.59	1.20
13	Control	71	M		12	30	0	0.06	4.25	-0.81	1.51	1.20
14	Control	60	F		12	30	0	-0.30	4.64	1.23	0.88	1.35
15	Control	65	M		16	30	0	1.52	5.53	1.20	-0.23	0.87
16	Control	87	M		8	29	0	2.81	-0.70	0.27	0.36	2.47
17	Control	63	M		16	30	0	1.71	5.91	0.01	0.82	-0.10
18	Control	57	F		16	29	0	0.10	2.75	1.28	1.93	0.59
19	Control	61	M		17	29	0	0.39	4.26	1.22	0.02	0.86
20	Control	85	M		12	29	0	0.73	1.48	0.07	0.31	-0.61
21	Control	76	M		5	28	0	0.96	3.51	1.26	1.33	2.70

Table S4. Detailed information of viruses used in this study

Figure	Virus	Titer (GC/ml)	Volume (uL)	Total amount (GC)
1C	Adeno-GFAP-GFP	3.34X10^9	1	3.34X10^6
1H	Adeno-GFAP-GFP	3.34X10^9	2	6.68X10^6
1M, LEFT	Adeno-GFAP-GFP	3.34X10^9	2	6.68X10^6
1M, RIGHT	Adeno-GFAP-GFP	3.34X10^9	1	3.34X10^6
	AAV-GFAP-cre	7.94x10^12	0.5	3.97x10^9
	AAV-pSico-MCT1shRNA -GFP (AAV-pSico-shScram-GFP)	1.85x10^13 GC/ml (3.06x10^13 GC/ml)	0.5	0.93x10^10 (1.53x10^10)
4	AAV-GFAP-cre-mCherry	2.61x10^13 GC/ml	0.5	1.31x10^9
	AAV-pSico-MCT1shRNA -GFP (AAV-pSico-shScram-GFP)	1.85x10^13 GC/ml (3.06x10^13 GC/ml)	0.5	0.93x10^10 (1.53x10^10)
S1E, I	Adeno-GFAP-GFP	3.34X10^9	2	6.68X10^6
S2D	AAV-GFAP-cre-mCherry	2.61x10^13 GC/ml	0.5	1.31x10^9
	AAV-pSico-MCT1shRNA -GFP (AAV-pSico-shScram-GFP)	1.85x10^13 GC/ml (3.06x10^13 GC/ml)	0.5	0.93x10^10 (1.53x10^10)
S2G, J	Adeno-GFAP-GFP	3.34X10^9	1	3.34X10^6
	AAV-GFAP-cre	7.94x10^12 GC/ml	0.5	3.97x10^9
	AAV-pSico-MCT1shRNA -GFP (AAV-pSico-shScram-GFP)	1.85x10^13 GC/ml (3.06x10^13 GC/ml)	0.5	0.93x10^10 (1.53x10^10)
S6, S7	AAV-GFAP-cre-mCherry	2.61x10^13 GC/ml	0.5	1.31x10^9
	AAV-pSico-MCT1shRNA -GFP (AAV-pSico-shScram-GFP)	1.85x10^13 GC/ml (3.06x10^13 GC/ml)	0.5	0.93x10^10 (1.53x10^10)

Original blots and gel images

Supplementary Figure 1

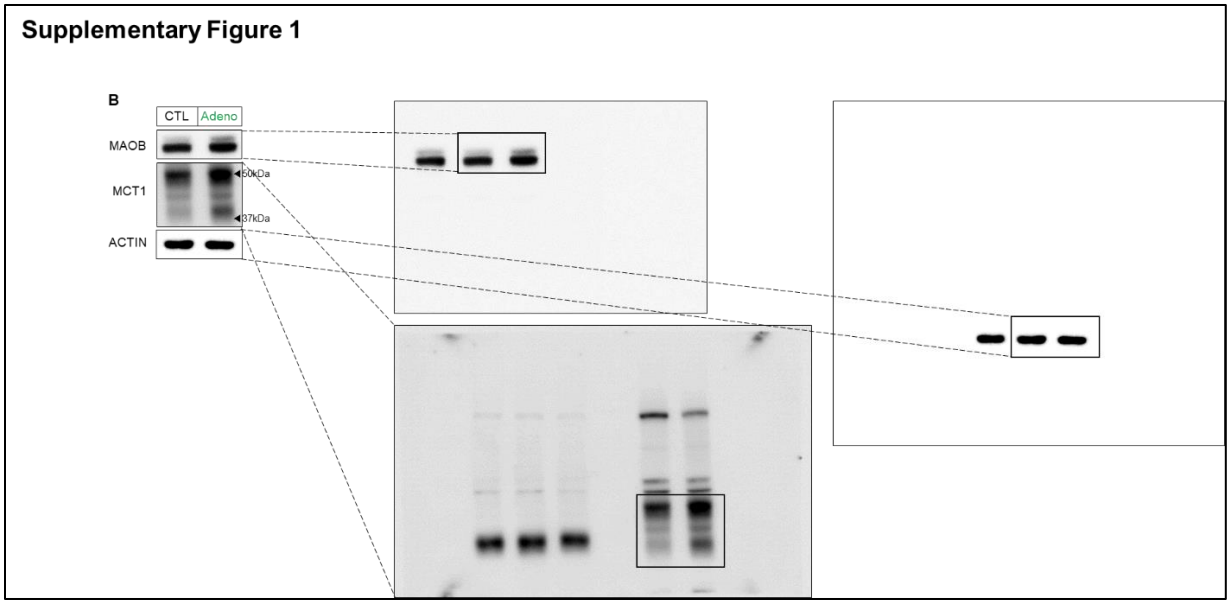

Supplementary Figure 2

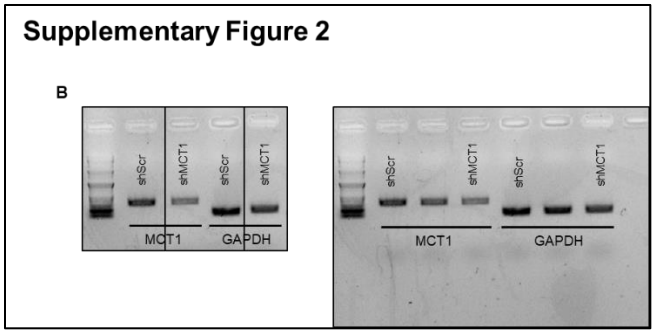

Supplementary Figure 3